The current state of Lake Dålk (Larsemann Hills, East Antarctica)

Anastasiia Sukhanova [a,*], Dmitry Bantsev [b], Sergey Popov [c,b], Alina Boronina [d,b], Egor Shimanchuk [e], Sergey Polyakov [e]

[a] First Geotechnical Company LLC (FGC), 4 Kantemirovskaya Str., St Petersburg, 194100, Russia
[b] St Petersburg State University (SPbU), 7–9 Universitetskaya Emb., St Petersburg, 199034, Russia
[c] Polar Marine Geosurvey Expedition JSC(PMGE), 24 Pobeda Str., Lomonosov, St Petersburg, 198412, Russia
[d] State Hydrological Institute (SHI), 23 2nd line Vasilyevsky Island, St Petersburg, 199004, Russia
[e] Arctic and Antarctic Research Institute (AARI), 38 Bering Str., St Petersburg, 119397, Russia

ARTICLE INFO

ABSTRACT

The study focuses on the current state of englacial Lake Dålk (Larsemann Hills Oasis), which was completely devastated in January 2017 by a catastrophic outburst and formed again in February 2020. A set of works including ground-penetrating radar (GPR) profiling, geodetic survey, core drilling, thermometric measurements and isotopic analysis was performed. As a result, new data were obtained about the modern boundaries of the reservoir, ice thickness and depths, as well as about the peculiarities of freezing of the lake after re-formation. Based on the field data obtained, one-dimensional mathematical modeling of Lake Dålk freezing was carried out, the results of which showed further scenarios of its evolution.

1. Introduction

Lake Dålk is located in the eastern part of the Brokness Peninsula (Larsemann Hills Oasis, East Antarctica) near the Russian Progress-1 field base. From a hydrological point of view, Lake Dålk is of particular interest because it is an englacial lake. The bottom of the lake is located inside the Dålk outlet glacier in the area of its adjoins the rocks of the oasis (Fig. 1). Despite years of knowledge about the Larsemann Hills hydrographic system (Gillieson et al., 1990; Gasparon et al., 2002; Kaup and Burgess, 2002; Shevnina and Kourzeneva, 2017), the existence of an englacial lake only became known in January 2017. At that time, a vast depression of about 40.260 m^2 and 183 × 220 m in size was formed on the site of the reservoir (Popov et al., 2017). The formation of the depression was preceded by an outburst of Boulder and Ledyanoe lakes, the water from which rushed through surface and intraglacial channels in the Dålk Glacier to the englacial reservoir. There was an overflow of Lake Dålk and its further drainage into Prydz Bay (Boronina et al., 2021).

Three years later, in January 2020, there was a second outburst of Boulder and Ledyanoe lakes. As a result, the depression was filled with water and in 14 days Lake Dålk was completely restored (Boronina, 2022). In early February 2020, the newly formed body of water was covered with ice and has been visually dormant since then (Fig. 2a and

b). A detailed description of the Boulder-Ledyanoe- Dålk lakes system was given based on studies conducted at the site from 2017 to 2020 during the seasonal work of the 63, 64, and 65 Russian Antarctic Expeditions (Boronina et al., 2021). Based on the simulation results, a re-outburst of the englacial Lake Dålk should be expected.

Monitoring the current state of Lake Dålk is extremely important. The consequences of outburst floods on the Brokness Peninsula of the Larsemann Hills poses a threat to the logistic routes and infrastructure of the Russian (RAE) and Chinese (CHINARE) Antarctic Expeditions (Popov et al., 2018). Channels in snow-ice dams formed during outbursts of Progress and Boulder lakes make it difficult for vehicles to move around the oasis (Grigoreva et al., 2021; Boronina, 2022). The formation of a depression at the Lake Dålk site in January 2017 also led to the destruction of the road between Progress (Russia), Zhongshan (China) stations and the airfield (Sukhanova et al., 2020). After the new Lake Dålk was frozen again, traffic also travels on the surface of lake during the Antarctic winter and spring. Therefore, the study of its current state is necessary to ensure the safety of transport operations and to understand the processes of formation and evolution of englacial water bodies.

This article presents the results of surveys in January 2021 (66th RAE) and January 2023 (68th RAE). By January 2023, three years had passed since the formation of Lake Dålk at the site of the depression. The

---

* Corresponding author.
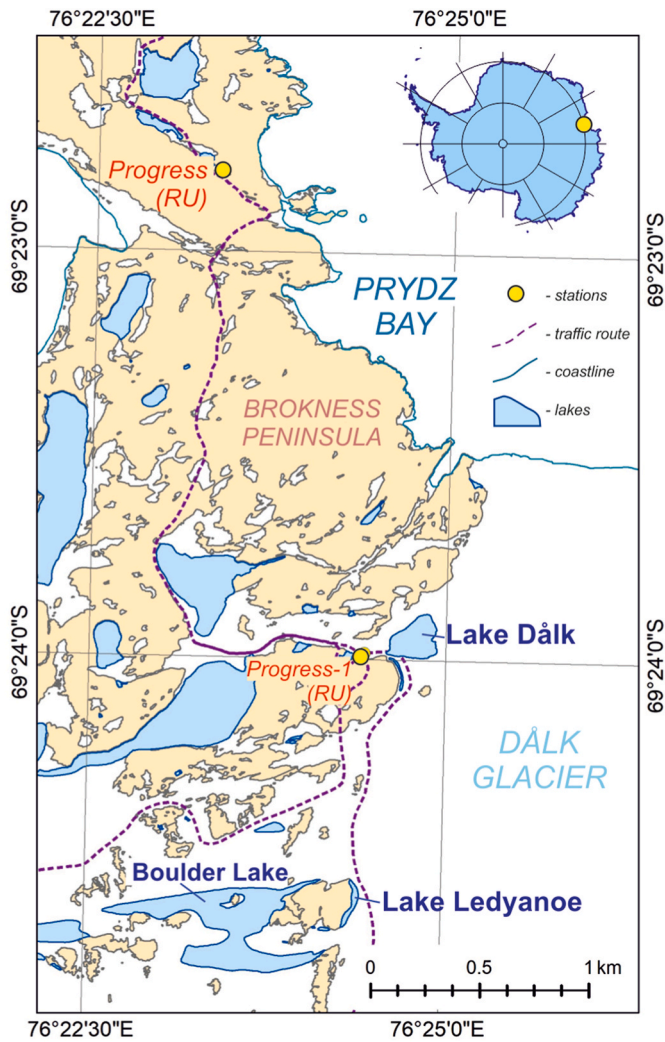 E-mail address: suhanova.anastassiya@yandex.ru (A. Sukhanova).

Fig. 1. Scheme of the work area on the territory of the oasis.

fieldwork was carried out in the Dålk Glacier area near the Progress-1 field base on the surface of the newly formed ice of the reservoir. Based on the work results, a description of the current state of Lake Dålk is given and possible future scenarios for its development are demonstrated.

2. Methods and data

This section presents the methods of the field studies and the modeling of Lake Dålk evolution. The field research includes a GPR survey, test drilling to determine ice thickness and water depth, ice core drilling and thermometric observations. The position of the profiles and research points are shown in the scheme in Fig. 3. The methodology of the modeling includes a description of the mathematical model based on the solution of the one-dimensional Stephan multiphase problem, and the software implementation of the modeling algorithm.

2.1. Field works

GPR profiling was performed across the contour of the englacial reservoir at the time of its freezing in February 2020. During the study period, 3.1 km of 900 MHz antenna routes and 3.0 km of 38 MHz antenna routes were done. The selected frequency allowed us to study Lake Dålk in its near-surface part and to get ice thickness information, and also to estimate the depth of the reservoir. The profiles shown in Fig. 3. GPR data processing consists of subtracting the direct pass signal and adjusting the amplitudes of the recorded wavefield to increase the signal-to-noise level. Subsequently, the depth relative to the surface was determined for each boundary identified on the GPR transects.

The test drilling measurements were carried out to study the thickness of the lake ice cover and its depth in two stages during the season of the 66th and 68th RAE. Reference drilling in January 2021 was performed at 13 locations and drilling in January 2023 was conducted at 6 locations (Fig. 3).

The structure and physical properties of the ice were studied based on ice core drilling. Core sampling allowed us to determine the density of ice ρ (kg/m^3) as the ratio of the mass m (kg) of each fragment to their volume V (m^3). Immediately after core sampling, temperature measurements were taken every 5–10 cm of the core. In addition to density analysis, ice samples were taken from ice core to determine the paired isotopic characteristics of oxygen $\delta^{18}O$ and deuterium δ^2H. Their correlation reflects the peculiarities of lake ice formation and can provide additional information about the processes occurring in the lake after its formation in 2020. The isotope composition measurements were performed at the Laboratory of Climate and Environmental Change (LICOS) of the AARI. Beyond that, part of samples was analyzed for NaCl (ppm) and KCl (μCm) concentrations.

The thermometric observations were carried out to study the temperature regime of the englacial reservoir. For this purpose, the thermometric string was lowered along the vertical profile from the surface to the bottom at a point with a depth to the lake bottom mark, equal to 26.5 m. Sensors that record the temperature of the water are placed every meter of the string in an upright position. The temperature was measured once a minute with a sampling rate of 0.01 °C between 06:40
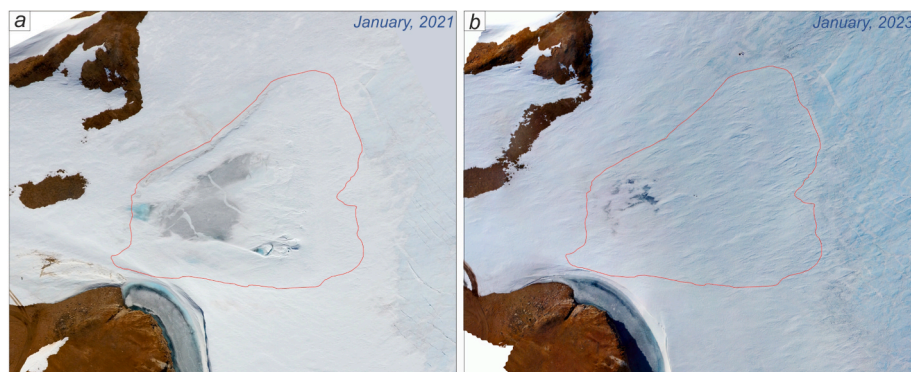

Fig. 2. Overview of the study area: a – surface of Lake Dålk in January 2021 (photo by S. Polyakov), b – surface of Lake Dålk in January 2023 (photo by D. Emelyanov).
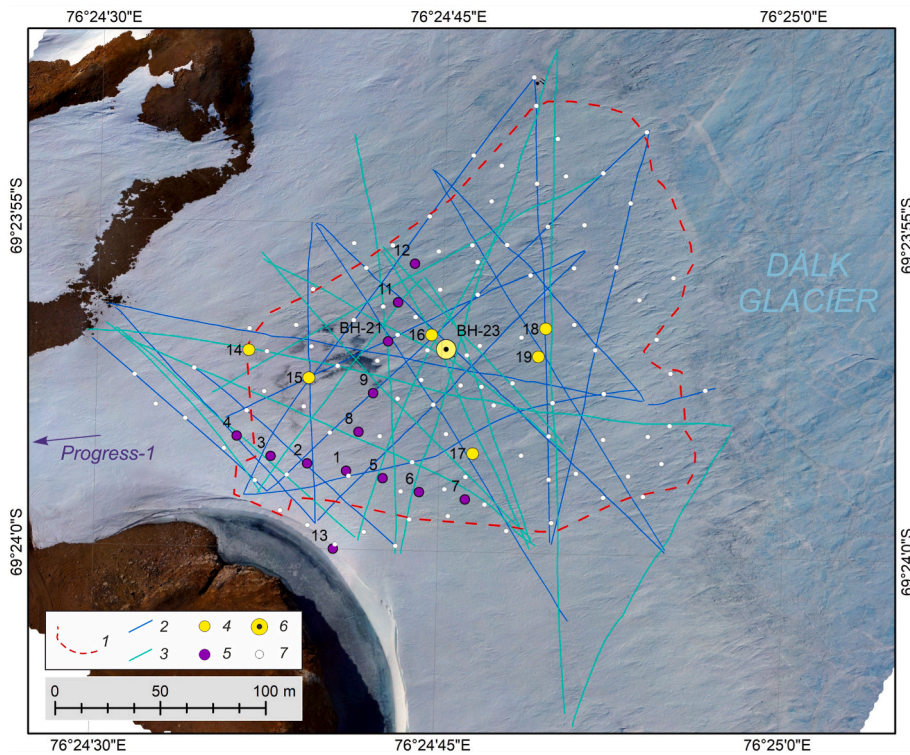
Fig. 3. Field studies in the Lake Dålk area during the season of the 66th and 68th RAE:1–Lake Dålk contour at the time of its formation in February 2020; 2–900 MHz GPR survey in January 2023; 3–38 MHz GPR survey in January 2023; 4 – test drilling in January 2021; 5 – test drilling in January 2023; 6 – core sampling and thermometric string installation point in January 2023; 7 – GNSS measurement points in January 2023.

UTC on January 23, 2023, and 08:26 UTC on January 25, 2023 (2 days).

GPR routes, drilling points, thermal sensors and measurements of absolute heights were carried out with GNSS positioning and also with help of Garmin transceiver. The limits of acceptable absolute error of measurements for GNSS were ±24–33 mm in plan and ±45–54 mm in height, for Garmin were ±3.65 m.

All steps of the performed studies are presented in the flowchart in Fig. 4. The described field methods allowed us to obtain data for further mathematical modeling of Lake Dålk changes.

2.2. Kinematic model

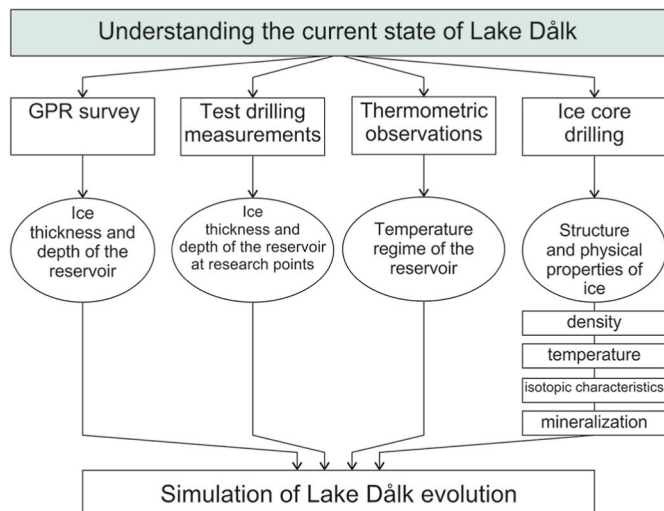To interpret GPR data, information on the electromagnetic wave

Fig. 4. The flowchart representing a process of studying.

velocity ϑ (m/s) or dielectric permittivity ε (units) for the media is needed. This allows for switching from temporary GPR sections to depth sections. For each of the layers identified by the GPR data, information about the kinematic characteristics was determined based on field measurements and theoretical calculations.

The results of ice thickness h measurements performed near the GPR routes in test drilling 14–17 (Fig. 3) allowed us to estimate the dielectric permittivity ε for the layer of surface snow and the cover ice thickness, according to the expression:

$$h = \frac{ct}{2\sqrt{\varepsilon}} \tag{1}$$

where c – the speed of light in vacuum, m/s, t – the arrival time of the reflected wave according to GPR data, s. The value of dielectric permittivity for snow was determined at the level of 1.9 units, for lake ice was 3.1 units, which corresponds to electromagnetic wave velocities of 217.5 m/μs and 170.3 m/μs, respectively. In the case of considering the cover of an intraglacial reservoir without separation into separate layers, the effective value ε was 3.1 units, and the electromagnetic wave velocity was 170.3 m/μs.

It should be noted that the boundary between the ice lenses and the underlying lake ice was not detected during the reference measurements of ice thickness, and therefore it is impossible to obtain data on the kinematic characteristics of the substance composing the lenses from the drilling data. However, an informative way to obtain data on electromagnetic wave propagation velocities is the method of determining dielectric permittivity from diffracted wave time curves (Vladov and Starovoitov, 2004; Glazovsky and Macheret, 2014; Popov, 2017). The reason for their formation on the wavefield of GPR sections is the presence of local inhomogeneities in the medium, which are secondary sources of oscillations. Since diffracted waves characterize the velocities of electromagnetic wave propagation in the medium above the diffraction object, attention was paid to diffractions at the interface between lenses and lake ice. The values of dielectric permittivity were calculated

from the GPR data by 8-time curves of the diffracted waves. The value of ε permeability for these time curves varies in the range from 3 to 3.2 units, which corresponds to the velocity of propagation of electromagnetic waves 167.8–173.1 m/μs. When recalculating GPR-time sections into depth sections, an averaged value of ε equal to 3.1 was taken for lenses, which corresponds to the electromagnetic wave propagation velocity of 170.3 m/μs.

For the water column, comparing the data of water depth measurements and the arrival time of reflections from the lake bottom, the dielectric permittivity was determined at 88.5 units, which corresponds to the wave propagation velocity of 31.9 m/μs. The water temperature, according to the thermometric measurements in BH-23, ranges from −0.01 to 0.05 °C. According to Chernyak (1987), the value of the dielectric permittivity of water depends on temperature according to the expression:

$$\varepsilon = 80/((1 + 0.0048(T - 20)))\tag{2}$$

where T is water temperature, °C. At the above temperature range, the dielectric permittivity will be 88.5 units, and the wave velocity is 31.9 m/μs, which coincides with the calculations from the reference drilling data.

Summarizing the results, the value of dielectric permittivity for snow is determined at the level of 1.9 units, for lake ice is 3.1 units, for ice lenses is also taken 3.1 units. For the water column the effective value ε is 88.5 units.

2.3. Mathematical model

2.3.1. Parameter setting

As part of this work, we will simulate the evolution of Lake Dålk. According to the results of field studies, the depression that existed at the site of Lake Dålk for three years was filled with water on January 25, 2020, as a result of the repeated drainage of the Bolder and Ledyanoe lakes (Boronina et al., 2021). After filling the lake, part of the water began to spill over the surface of the glacier in a northeasterly direction, and water migrated from the reservoir through a system of crevasses into its strata at a distance of about 400 m. Just a few days later, on February 1, 2020, Lake Dålk was already covered with a thin ice. In this regard, the starting point for the beginning of the modeling is the point in time t_o January 25, 2020, when Lake Dålk was overflowed. Then, on January 4, 2021, at the coordinates 69°23′56.8″ S and 76°24′42.5″ E, well *BH-21* was drilled (Fig. 3), where the water depth of Lake Dålk and the ice thickness above it were measured. This point in time is t_1. The moment of time t_2 will be January 25, 2023, when well *BH-23* was organized 27 m east of the last point (Fig. 3). A core of lake ice was taken in the *BH-23*, and the thickness of snow, ice and water and the vertical change in temperature in all media were measured. Both wells *BH-21* and *BH-23* are located approximately in the central part of the reservoir, at a distance of about 80 m from the shoreline to the north and south, and a distance of about 100 m from the western and eastern shores (Fig. 3). Since these values are several times greater than the water depth of the reservoir and more than an order of magnitude greater than the ice thickness at the time of measurement, the influence of edge parts on the heat and mass transfer process at the point selected for the calculation is minimal. It follows that the use of a one-dimensional model to assess the development of the processes under discussion in the framework of the task is justified.

2.3.2. Description of the mathematical model

Thus, the mathematical model is based on the solution of the one-dimensional multiphase Stefan problem. At the initial moment of time t_o, the studied system consists of two media: the water Ω_W and the underlying ice layer Ω_G. Between them, there is a phase boundary Γ_{WG}, $\Gamma_{WG} = \Omega_W \cap \Omega_G$, which can move up or down during the freezing–melting processes (Fig. 5).
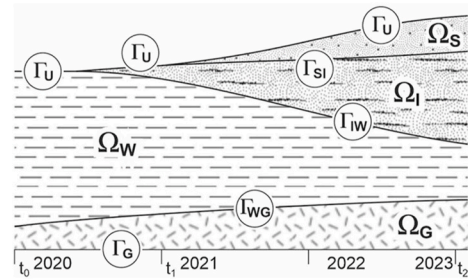

Fig. 5. The idealized system considered in the mathematical model.

We set the temperature distribution in Lake Dålk and the underlying glacier as the initial conditions. Assuming that the water entered the depression by advancing through the glacier, it is logical to assume that at time t_o the water temperature in Lake Dålk θ_W is about to the phase transition temperature θ_F. This is confirmed by thermometry data (Fig. 8, section g). The initial temperature distribution in the underlying glacier θ_G is set equal to the permafrost temperature on the Larsemann Hills $\overline{\theta}_P$, $\overline{\theta}_P = -8.5°C$ (Vieira et al., 2010). The thickness of the glacier (*T*) under Lake Dålk at the estimated point is unknown. However, according to the radar data obtained during the season of the 32nd Soviet Antarctic Expedition (1985/86), it may be several tens of meters (Popov, 2022). For certainty, we take it to be $T = 20$ m.

We designated the upper boundary as Γ_U and set the condition of heat exchange with the atmosphere. The equations of state for calculating the effective coefficients for this boundary condition with respect to the Larsemann Hills are presented in (Popov et al., 2023).

The remaining boundary conditions are less obvious, so we introduce them in more detail. At the lower boundary of the glacier Γ_G, we set the value of the geothermal heat flux Λ_o. We take it to be $\Lambda_o = 55.4$ mW/m², as this value is presented in (Martos et al., 2017) for the area closest to the Larsemann Hills. For certainty, let us direct the z-axis upward, aligning the origin of coordinates with the boundary Γ_G (Fig. 5).
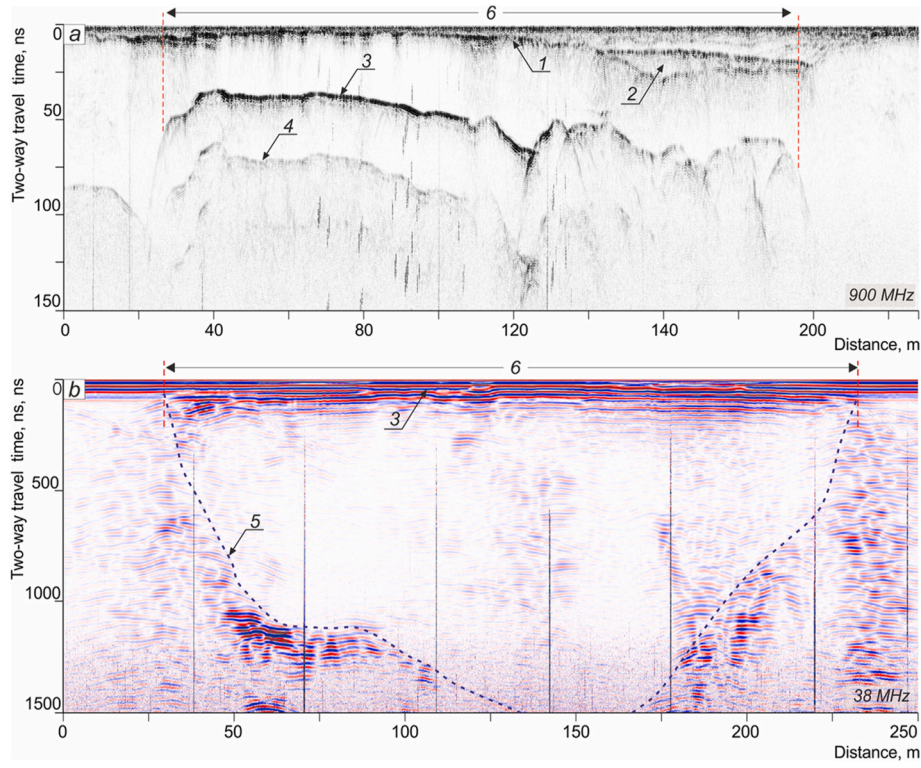
After a while, the water in Lake Dålk will begin to freeze, and a gradually thickening layer of ice Ω_I will form on the surface. Due to changes in air temperature, solar radiation, and the Sun's height above the horizon during the day and from season to season, a layer of meltwater can form on the ice surface. This process causes the appearance of a layered structure containing ice and melt water. This is what was observed on the frozen surface of Lake Dålk during the summer field season of 2021. These layers of ice and meltwater can form and disappear over time. The boundaries between them Γ_{WI} are phase boundaries.

In addition, snowfall periodically fell on the surface of ice or meltwater Γ_U during the estimated time. The analysis of meteorological data presented in (Popov et al., 2023) shows that they fall quite evenly throughout the year. If they hit the surface of the meltwater, they raise it's level by an appropriate amount. Falling on the ice, they form a layer of snow Ω_S, the thickness of which on one side gradually increases, and on the other side decreases as a result of compaction and blowing away.

The concept of the stated mathematical model is given by the equations:

$$\rho_I c_I \frac{\partial \theta_I}{\partial t} = \lambda_I \frac{\partial^2 \theta_I}{\partial z^2}, z \in \Omega_I$$

$$\rho_W c_W \frac{\partial \theta_W}{\partial t} = \lambda_W \frac{\partial^2 \theta_W}{\partial z^2}, z \in \Omega_W$$

$$\rho_S c_S \frac{\partial \theta_S}{\partial t} = \lambda_S \frac{\partial^2 \theta_S}{\partial z^2}, z \in \Omega_S\tag{3}$$

$$\lambda_I \frac{\partial \theta_I}{\partial z}\bigg|_{\Gamma_{IW}} - \lambda_W \frac{\partial \theta_W}{\partial z}\bigg|_{\Gamma_{IW}} = q_F \rho_I \frac{dz}{dt}\bigg|_{\Gamma_{IW}}, \lambda_I \frac{\partial \theta_G}{\partial z}\bigg|_{\Gamma_{WG}} - \lambda_W \frac{\partial \theta_W}{\partial z}\bigg|_{\Gamma_{WG}} = q_F \rho_I \frac{dz}{dt}\bigg|_{\Gamma_{WG}}$$

Fig. 6. GPR research at the Lake Dålk area:a –GPR time-section at 900 MHz; b –GPR time-section at 38 MHz:1– boundary between snow and lake ice; 2 – lens of frozen ice; 3 – boundary between lake ice and water; 4 – multiple waves; 5 – reservoir bed; 6 – reservoir boundaries.

$$T_I = T_W \frac{\rho_W}{\rho_I}, \theta_I(z)|_{\Gamma_{IW}} = \theta_W(z)|_{\Gamma_{IW}} = \theta_F$$

$$\lambda_S \frac{\partial \theta_S}{\partial z}\Big|_{\Gamma_{SI}} = \lambda_I \frac{\partial \theta_I}{\partial z}\Big|_{\Gamma_{SI}}, \lambda_j \frac{\partial \theta_j}{\partial z}\Big|_{\Gamma_U} = \alpha_E(\theta_{j0} - \theta_E), j = S, W, I;$$

$$\lambda_I \frac{\partial \theta_I}{\partial z}\Big|_{\Gamma_G} = \Lambda_0, \theta_G(z)|_{t=0} = \overline{\theta}_P, \theta_W(z)|_{t=0} = \theta_F$$

where ρ_I and ρ_W is the density of ice and water, respectively; λ is the thermal conductivity of the medium; c is its specific heat capacity. These values for ice and water are known: $\lambda_I = 2.22$ W/(m°C); $\lambda_W = 0.569$ W/(m°C); $c_I = 2.060$ kJ/(kg°C); $c_W = 4.212$ kJ/(kg°C). The thermal conductivity coefficient of snow λ_S depends on its density ρ_S. For the calculations, we will take the ratio successfully used for the Arctic and mountain glaciers (Osokin et al., 1999; Sosnovsky, 2006):

$$\lambda_S = 9.165 \times 10^{-2} - 3.814 \times 10^{-4} \rho_S + 2.905 \times 10^{-6} \rho_S^2 \quad (4)$$

In articles (Osokin et al., 1999; Sosnovsky, 2006), the specific heat capacity of snow c_S is take to be $c_S = 2100$ J/(kg°C). Also in (1) q_F is the specific heat of fusion ($q_F = 332$ kJ/kg); α_E and θ_E are the effective values of the heat transfer coefficient and ambient temperature, which are described by the equations of state. These equations take into account humidity, atmospheric pressure, cloud cover, and the height of the Sun above the horizon. This relationship, as well as the meteorological data that comprise it, are discussed in detail for the Larsemann Hills in (Popov, et al., 2023).

The above problem was solved numerically. For its implementation, we used an implicit finite-difference scheme with a variable step followed by the use of the elimination method (Samarsky and Vabishchevich, 2003). The difficulty of the software implementation was solving the Stephan multiphase problem since new layers could both form and disappear under the influence of external conditions. This was implemented through a specially designed algorithm. The idea of this algorithm is as follows. We will assume that the external conditions are such that the lake ice begins to melt on contact with the atmosphere. This means that the ice medium will be divided into two parts in the model. The lower part of the medium will retain the old properties, while the upper part will be characterized by new ones. The same thing happens algorithmically. We set some threshold layer thickness dT. If the thickness of the initial medium is T, then after subdivision, the thickness of the lower layer becomes equal to T-dT, and the upper one is dT. The number of points in each layer, including newly formed ones, is the same and equal to N. We perform a linear interpolation of all parameters (density and temperature) of the initial medium into two new layers to ensure correctness. In addition, the Stefan condition is observed at the boundary of the layers.

A similar idea is laid down on the border between lake water and ice at the bottom of the lake. Abstractly, we will assume that the external conditions are such that the water cools and begins to freeze at the bottom, turning into ice. In this case, if the layer thickness becomes less than the threshold value dT, it is absorbed by the adjacent layer. In this case, the thickness of the ice medium increases. For the correct merging of layers, we perform a linear interpolation of their parameters.

Another example is when a layer disappears due to the simultaneous influence of two adjacent layers. For example, the freezing of a glacial lake. In this case, the ice layers are combined, and their thickness increases by the value of the intermediate layer. Parameter interpolation is again needed.

3. Results

3.1. Structure features of the glacier in the Lake Dålk area

Based on the results of the GPR studies, the environmental model at the Lake Dålk area was determined to be four-layered. Its main components from the surface are atmospheric snow, lenses of frozen ice, lake ice, and the water column. Examples of GPR time-sections obtained by
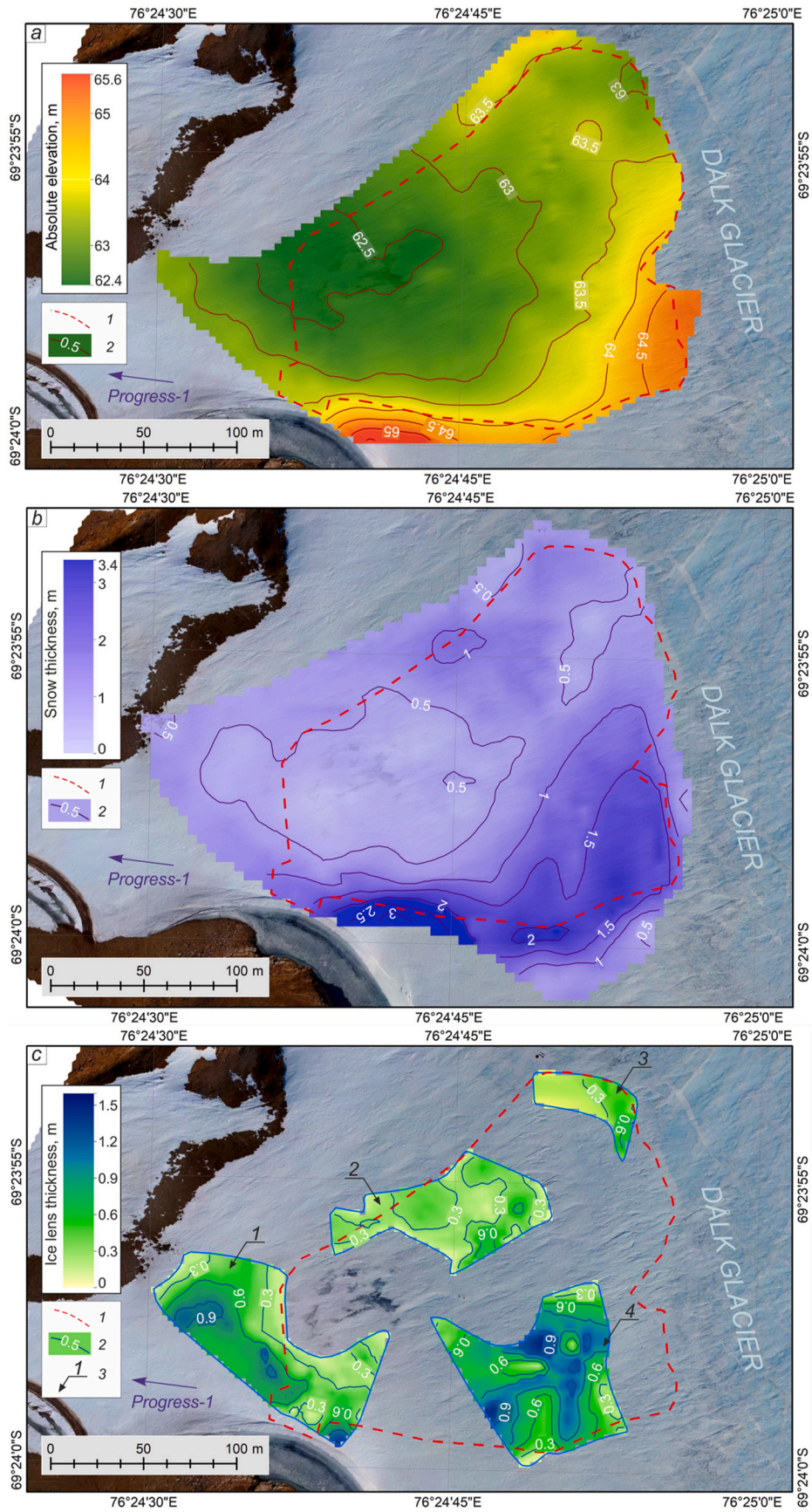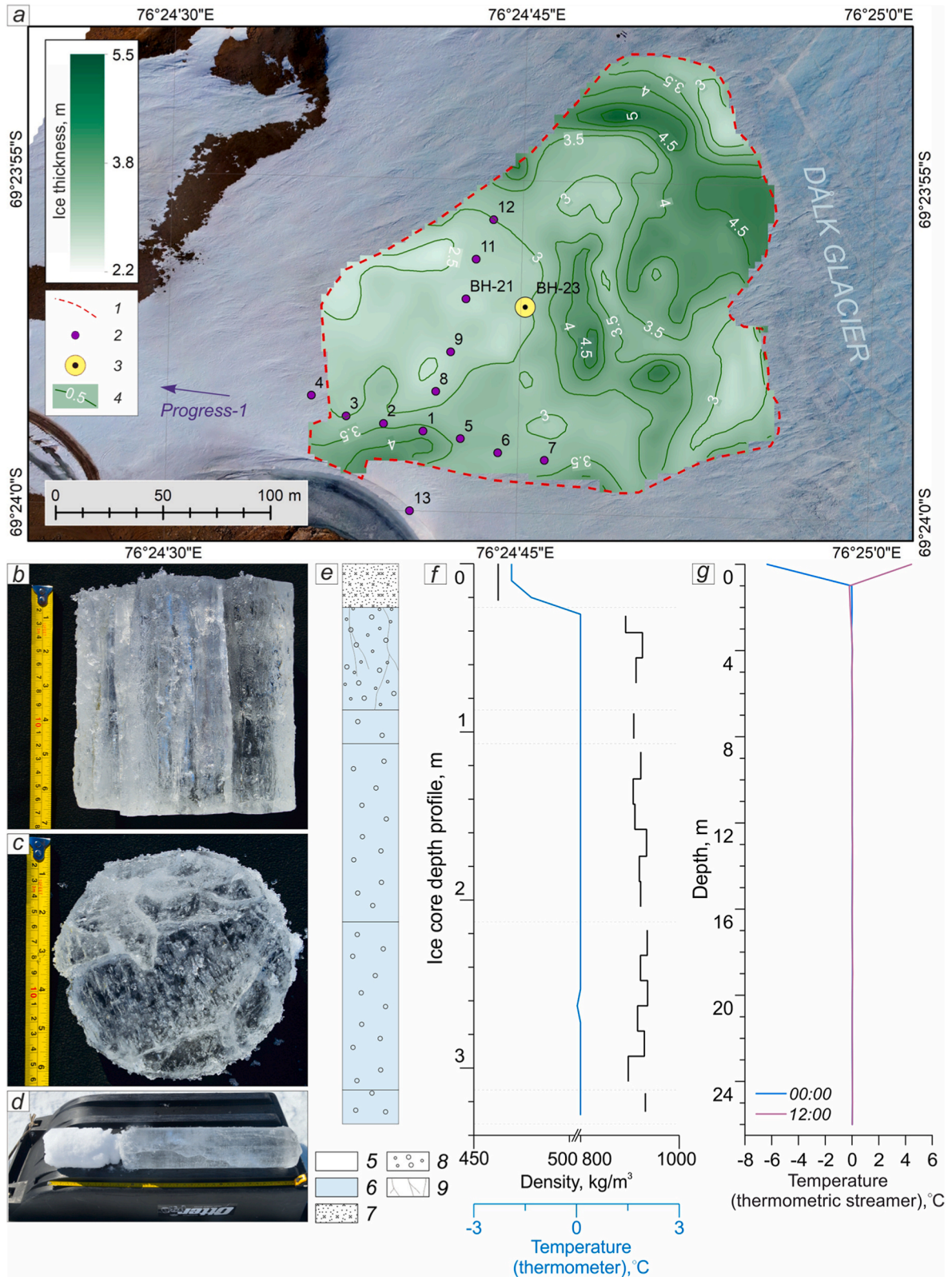
A. Sukhanova et al.

Fig. 7. Peculiarities of the structure of the near-surface part of Lake Dålk:a – scheme of surface topography; b – scheme of snowfall capacity, c – scheme of infiltration ice lens capacity:1 – water body boundary; 2 – isolines; 3 – lens number.

Fig. 8. Features of lake ice structure: a – diagram of lake ice thickness; b, c – structure of lake ice samples, d – stratigraphic core column; e – density and temperature profiles within the core; f – temperature profile at the point of thermometric string installation; g – temperature distribution in well BH-23 on January 25, 2023 at 00:00 and 12:00. 1 – Lake Dålk contour; 2 – control drilling points in January 2021; 3 – core sampling point and thermometric string installation; 4 – isolines; 5 – snow; 6 – ice; 7 – snow precipitation; 8 – air inclusions; 9 – crevasses forming in the near-surface part of the ice cover.

probing at 900 MHz and 38 MHz are shown in Fig. 6.

The time section obtained at 900 MHz characterizes the structure of the lake cover. There is no direct wave on the obtained section due to the filtering procedure. In the upper part of the section, there is an extended contrasting boundary *1*, corresponding to the division between snow sediments and ice. Locally, lenses *2* between sediment and ice were identified within the reservoir. During fieldwork, the presence of melt-water at boundary *1* was noted, so lenses *2* probably correspond to ice-freezing areas on top of lake ice.

Further, a contrast reflection *3* at the boundary of the lake ice and water is clearly recorded, accompanied by the formation of a multiple wave *4*. Moving along the profile the intensity of the reflected signal *3* decreases due to scattering of the signal on a more relief border.

At the arrival time of the reflected wave, equal to 150 ns, the electromagnetic signal attenuates, propagating in the water column of Lake Dålk. Boundary *5*, corresponding to the bottom of Lake Dålk, was obtained by probing at 38 MHz within the registration window of 0–1600 ns. The lake retained the configuration of the failure formed after the breach. The boundaries of the bed closer to the surface are sub-vertical.

3.2. Lake configuration

In addition to obtaining information about the features of the glacier structure at the Lake Dålk site, GPR data also allowed estimating the change in the boundaries of the water body compared to its configuration at the time of lake formation in January 2020. After filling the northern and eastern parts of the dip with water, the newly formed water body retained the contours of the depression. However, the spill in the southern part of the reservoir slightly changed the boundaries of the reservoir. As a result of water overflow through the snowy bridge, Lake Dålk connected to the cave reservoir. The results of ice thickness and depth measurements of Lake Dålk one year after its formation demonstrate a change in the reservoir boundaries. The most interesting from this point of view are the measurements in test points 4 and 13 (Fig. 3). Drill reference point 4 is located in the reservoir spill area on the west side. At this point, the ice thickness reached values of more than 3.5 m, no water was recorded at the drilling site. In this case, at the nearest measuring point No. 3 within the reservoir, the ice thickness was 1.65 m. Based on this, it was concluded that a year later the water layer at the site of the spill had frozen over completely.

In the southern part, drilling was performed at point 13 at the connection between Lake Dålk and the cave reservoir. According to the measurement results in January 2021, the thickness of the overlapping ice of the reservoir was 2.5 m, the depth of the reservoir on the bridge was 13.5 m. On this basis, it can be assumed that a year after its formation, Lake Dålk and the cave reservoir also represented a single system.

According to the GPR data at 900 MHz, the boundaries of Lake Dålk are fixed at the areas of sharp attenuation of electromagnetic wave *6* at the boundary between ice and water (Fig. 6a and b). The attenuation areas coincide with the position of the reservoir boundary after its formation in 2020. The change of boundaries is characteristic only for the site of the connection of Lake Dålk with the cave reservoir. GPR time-sections record the supposed location of the water body junction. The new boundaries in the area of the bridge between the lakes were used later for plotting and modeling.

3.3. Surface above the ice cover

Based on the results of the geodetic GNSS survey, a diagram of the relief of the day surface at the site within Lake Dålk was constructed, shown in Fig. 7a. In the central part of the reservoir, the relief is flat, and the height difference does not exceed 0.5 m. For the southern part of the work area, there is an increase in absolute elevations of about 3 m in contrast to the central area. The distribution of snowfall in the Lake Dålk area correlates with relief variability. The scheme of the snow thickness

covering the work site is shown in Fig. 7b. The central area of the works is characterized by the lowest accumulation of precipitation of the order of 0.5 m. The greatest snow thickness was recorded in the southern part of the site for areas with the largest elevation differences, from 1.5 to 3 m.

As the depth from the surface increases after the snow mass, infiltration ice lenses are revealed. We were able to trace their distribution from profile to profile using GPR data. As a result, the areas of the most intensive ice freezing were delineated in Fig. 7c. Their power varies from 0.1 to 1.6 m. The highest thickness was recorded within lens *4*, which is located in an area with more variable topography. Lens *1* is up to 1 m thick and is located at the site of the Lake Dålk spill in January 2020, and its formation is probably associated with the gradual freezing of the water layer at the site of the spill.

3.4. Ice cover

Based on the kinematic model, it was possible to estimate the ice thickness formed over the lake by the time of the described fieldwork. The final scheme of the cover ice thickness is shown in Fig. 8a. The thickness of the formed ice varies in the range from 2 to 6.2 m, with a tendency of increasing ice thickness in the marginal part of the reservoir adjacent to the Dålk Glacier. In the diagram in Fig. 8a, the ice thickness changes smoothly in the vicinity of the oasis spurs, but as we approach the Dålk Glacier, zones of ice thickness increase by up to 1 m at a distance of 10 m are recorded.

Ice core sampling, covering the reservoir at the failure site, was performed in its central part at the core point (Fig. 8a). The ice thickness at the core sampling point was 3.33 m. In the near-surface part of the ice cover, there was an insignificant accumulation of snow sediments – at the core sampling point, the snow sample thickness was 0.26 m. The fragment is characterized by a loose structure; ice crystals up to 2 mm in size are observed to be bound together closer to the 0.26 m mark. Further, lake ice, formed as a result of the gradual freezing of the reservoir, was recorded along the entire length of the sampled core. Lake ice is characterized by columnar vertical fragments (Fig. 8b, c and 8d) and the vertical direction of ice crystals. Ice within the first meter of the surface is more brittle, the samples are quite easily separated into individual columnar vertical specimens. With depth there is also a decrease in the number of air bubbles, the ice becomes more transparent. The snowfall density at 0–0.26 m from the surface is 462 kg/m^3. The frozen ice density within the depths of 0.26–3.33 m varies from 891 to 936 kg/m^3 (Fig. 8e and f).

According to the results of the thermometer measurements, the temperature on the surface of the water body ice cover is 2.1°C (Fig. 8g). At the "snow-ice" boundary at the transition to the lake ice the temperature increases to 0°C and stabilizes at this mark until the depth of 3.33 m. According to thermometric streamer measurements, the temperature values at depths of 1 m, 2 m, and 3 m from the day surface are 0.07 °C, 0.04 °C, and 0.00 °C, respectively, which confirms the validity of temperature determination using a thermometer.

The isotopic composition of the snow-firn layer of the upper part of the ice core differs from ice samples, $\delta^{18}O$ of snow is −24.38‰ (Fig. 9a). The upper part of the ice is affected by snow-firn meltwater refreezing. This refreezing is reflected in the lower values of the isotopic composition ($\delta^{18}O$ −20.25‰), but this refreezing affects only the upper number of centimeters of ice in the ice core. The isotopic composition of the ice from the depth 0.6 m displays low variability, $\delta^{18}O$ varies from −18.60 to −19.07‰. There is also no evidence of isotopic depletion. According to Gibson and Prowse (1999), a near-constant vertical profile indicates open-system fractionation, where water with constant d^{18}O circulates freely beneath the ice cover, and ice composition remains constant with time/depth. The slope between $\delta^{18}O$ and δ^2H defined by $\delta^2H = 7.964 \bullet \delta^{18}O + 0.802$ with R2 = 0.988 (Fig. 9b).

All ice samples generally fall close to the meteoric water line (MWL)
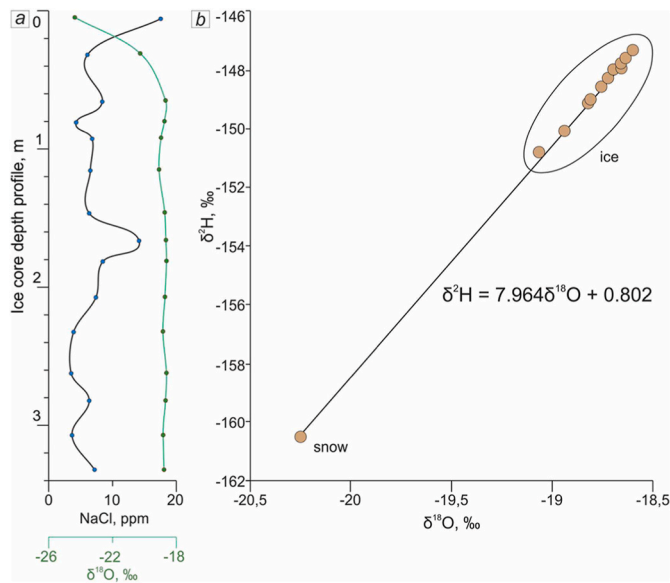
Fig. 9. Studies of the isotopic composition of lake ice:a – isotopic profile and mineralization profile; b – plot of $\delta^{18}O$ versus δ^2H for samples of ice in the core; 1 – snow; 2 – ice; 3 – snow precipitation; 4 – air inclusions; 5 – cracks forming in the near-surface part of the ice cover; 6 – ice sampling horizon for isotopic composition.

defined by $\delta^2H = 8\delta^{18}O + 10$ (Craig, 1961). In the case of congelation in close system conditions the slopes are less than 8 and generally ranging from about 5 to 7.

Therefore, according to the near-constant vertical isotopic profile, the lack of isotopic depletion, and the $\delta^{18}O$-δ^2H ratio, we suggest, that the formation of the depression ice cover was associated with near-constant feedwater source and open-system conditions.

3.5. Water depth

Based on the data from the 38 MHz GPR survey, as well as measurements of the water depth of the reservoir in January 2023, a bathymetric scheme of Lake Dålk was created (Fig. 10). It should be noted that due to hardware limitations, it was not possible to obtain reflections from the bottom of the reservoir over the entire area of Lake Dålk. According to the field results, the maximum water depth was 24 m.

In the eastern part of the reservoir, near the Dålk Glacier, according to GPR data, there was a significant decrease in the thickness of the water column, which is demonstrated in the diagram (Fig. 10). This is not characteristic of the configuration of the dip and does not coincide with the expected lake outline. The authors believe this may be due to the snow drift that existed in this part of the depression before it was filled with water in 2020. According to historic photos from January–February 2020, the outlines of the snow drift can be seen through the water column that filled the dip. It is possible that the incoming water could not completely melt the snow that was brought in.

3.6. Selecting snow accumulation parameters and testing the model for fit

It is necessary to know exactly how the layer of snow on its frozen surface was formed to model the process of changing the state of Lake Dålk. This is important as its presence significantly affects the heat transfer process. Unfortunately, there is no data on snow accumulation for the period from the formation of the reservoir (2020) to the present (2023) for the Lake Dålk area. According to data from the Progress meteorological station (Weather archive at Progress station (rp5.ru)), the average annual precipitation for the period from 2004 to 2022 is 232 mm of water equivalent. However, a different microclimate from the Progress station may well form in the area of the lake, as well as carry out wind transport. So the total accumulation there can be quite different. In this connection, it is possible to describe the pattern of snow accumulation in the Lake Dålk area only by indirect signs and separate measurements. Photographs and aerial photographs available to the authors, as well as 2021 field measurement data, indicate that the water area was virtually snow-free in the first year after the Lake Dålk restoration (2020–2021). We suggest that the reason for the lack of snow
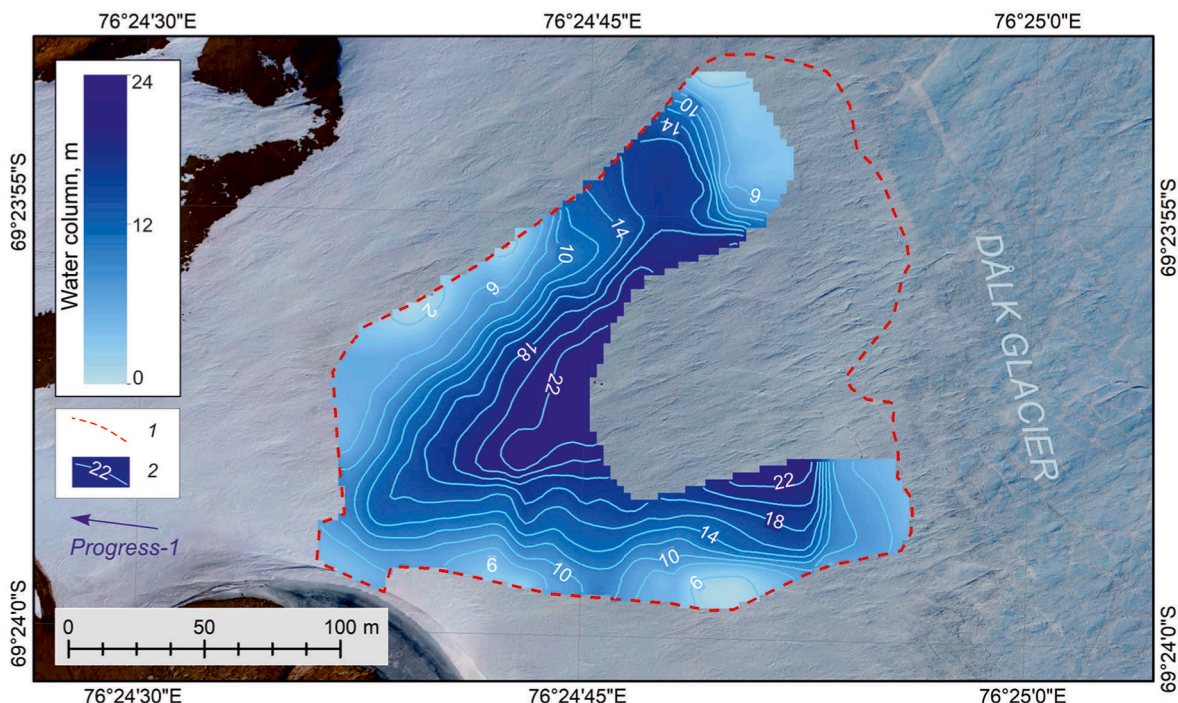
Fig. 10. Power diagram of the water column within the Lake Dålk:1 – contour of Lake Dålk; 2 – isolines.

accumulation on the frozen surface of Lake Dålk in the first year lies in the nature of its outburst. After the depression was filled with water, it overflowed and spread over the surface of the glacier with subsequent freezing, which, in turn, led to the uplift of its surface due to the difference in ice and water density. Therefore, the falling snow did not accumulate but was blown away by the wind. In addition, it was noted that the surface was heavily watered during the summer season, which probably also prevented snow from accumulating. In the next two years (2021/23), according to the core sampled at BH-23, the snow cover formed gradually. The density characteristics of the core (Fig. 8f) indicate that it consists of two environments. The upper part (first 0.26 m) is characterized by a density of 462 kg/m^3 and, according to isotopic analysis, was formed as a result of the metamorphism process of snowfall. The lower part is characterized by a density of about 919 kg/m^3 and a thickness of 3.07 m and also according to the results of isotopic analysis was formed in the freezing of lake water. The snow core is homogeneous in its structure (Fig. 8d and e). It lacks internal ice layers formed by periodic melting and freezing, which also indicates gradual snow accumulation from 2021 to 2023.

Based on the above, we divided the modeling into two parts. The first one is realized for the time interval [t_0, t_1], lasting 0.9466 yr, and we have calculated for *BH-21*. We guess that there was no snow layer at this point during the studied period (from January 25, 2021, to January 4, 2021). Having received the result of the calculation, we compare the measured values and the model ones. The correspondence of these values indicates the adequacy of the mathematical model used. After making sure that the model is fit, we implement the calculation of the calculation of the second part. We are modeling for the *BH-23* on the time interval [t_0, t_2], with a duration of 3.003 yr. In this case, in *BH-23*, set the patterns of changes in the thicknesses and densities of the snow-firn strata so that the measured values of the snow-firn strata and ice coincide within the accuracy with the model values.

Since the simulation is performed for different points, the depth of Lake Dålk at time t_0 in them will be different. For the calculation of heat and mass transfer, it has no decisive value, because, firstly, the thickness of the water layer is much greater than the damping depth of seasonal and daily fluctuations, and secondly, because with such a water layer the thermophysical processes occurring on the lake bottom cannot have a significant impact on its near-surface part. Nevertheless, the initial depth of the lake must formally be set to perform the simulation.

Let the position of the lake bed is constant in the time interval [t_0, t_2] for both points, because the obtained vertical temperature distribution indicates the absence of melting on the bed. Then we take as the initial depth of Lake Dålk at BH-21 the value of the water layer thickness measured in the borehole on January 4, 2021 (15.745 m) summed with the ice thickness (2.02 m) in terms of the water equivalent. If we take the average ice density to be $\rho_I = 919$ kg/m^3, based on core drilling data, then the depth of Lake Dålk at the time when it filled in 2020 is 17.61 m. By analogy and taking into account the accumulated snow with a density of 462 kg/m^3 we obtain the value of the lake depth at BH-23 at time t_0 equal to 26.14 m.

As mentioned, we first performed calculations on the time interval [t_0, t_1] for BH-21. At this stage, we have selected the parameters included in the equation of state for the boundary condition of heat exchange with the atmosphere so that the difference between the measured and calculated ice thickness was minimal. As a result of modeling, it was found that the best parameters are those used for thermophysical calculations in the Russian sector of the Arctic and the Svalbard Archipelago (Sosnovsky, 1984, 2006; Osokin et al., 1999). Under these parameters, the thickness of frozen ice over Lake Dålk during the calculation period was 2.01 m against 2.02 m obtained from in-situ measurements. These values coincide within accuracy. This means that the equations of state used, published in (Sosnovsky, 1984, 2006; Osokin et al., 1999), are also suitable for modeling in Antarctica, which demonstrates their universality. In addition, the calculations show that during this time there was ice freezing on the bottom of the lake, which

amounted to 0.35 m. The model showed adequacy.

We then calculated on the time interval [t_0, t_2] for point BH-23 with the above parameters. Describing the process of snow accumulation causes known difficulties, as in the absence of monitoring of snow accumulation and compaction during the year, this pattern is unknown. However, as indicated earlier, the obtained core allows making a reasonable assumption that it is homogeneous and the snow-firn strata were formed and compacted linearly. In this case, we set the increase in the thickness of the snow-firn strata according to a linear law in the interval [t_1, t_2] from zero to 0.26 m and its similar compaction from 110 kg/m^3 (Osokin et al., 1999; Sosnovsky, 2006) to the measured value 462 kg/m^3. Modeling showed that with the selected parameters, the calculated ice thickness over Lake Dålk in 2023 was 3.07 m, which fully corresponds to the measured value. Ice freezing at the bottom of the lake was 0.62 m. The slowing rate of ice build-up on the bottom is associated with a decrease in the temperature gradient in the underlying glacier due to the influence of water.

4. Discussion

4.1. Scenario calculations of the evolution of Lake Dålk for the next 5 years

Using the model presented above, consider the possible evolution of Lake Dålk for the next five years, i.e., until December 31, 2028. To do this, let us simulate three different scenarios for BH-23. All of them will start at time t_0 and will evolve until time t_2 as described in the previous section of the article. Then each of the three scenarios will be applied sequentially. According to the results of the earlier modeling, it was obtained that by 2023 at BH-23 ice freezing 0.62 m thick occurred on the lake bottom. In this connection, let us correct the depth of Lake Dålk at the initial moment by this value, i.e., let us set its initial depth equal to 26.76 m.

Following (Popov et al., 2023), to obtain data to calculate the effective coefficients included in the heat transfer equation, we perform averaging of air temperature and humidity, atmospheric pressure, wind speed, and cloud cover for the period from October 20, 2012, to May 5, 2023. At the same time for each day of the year, we obtain the average value of each of the meteorological parameters. Then we will apply them cyclically for calculations until December 31, 2028. The difference between the scenarios lies in the use of different patterns of changes in the thickness of the snow-firn layer, as well as its compaction.

The first scenario assumes that the thickness and density of the snow-firn strata will remain unchanged from 2023 to 2028. According to the results shown in Fig. 11a, the ice thickness over Lake Dålk at the calculated point increased to 5.85 m (ice growth since t_2 was 2.78 m). The freezing process occurs at a slower rate than was observed from 2020 to 2023 due to the presence of a snow-firn layer of constant thickness. A total of about 0.97 m of ice froze at the lake bottom. Thus, the total decrease in the thickness of the water layer was 6.82 m or slightly more than a quarter of its initial value.

The second scenario assumes a uniform increase in the thickness of the snow-firn strata with the same dynamics as in the time interval [t_1, t_2] and at a given density of 462 kg/m^3.

The simulation results are shown in Fig. 11b. As follows from their analysis, the ice thickness over Lake Dålk during the entire calculation period increased to 5.40 m, and the growth since the time t_2 was 2.33 m. The reservoir freezing rate is less than in the previous scenario, which is explained by the increase in the snow-firn strata throughout the calculation period. The increase in the snow-firn strata has led to the conservation of heat and, consequently, to a slowing of the process of ice freezing over the lake. At the bottom of the reservoir, a total of 0.97 m of ice froze, just as in the previous scenario. The total decrease in water depth was 6.37 m. Thus, since the initial point in time, the lake has frozen over by a little less than a quarter.

The third scenario assumes a uniform increase in the snow-firn strata
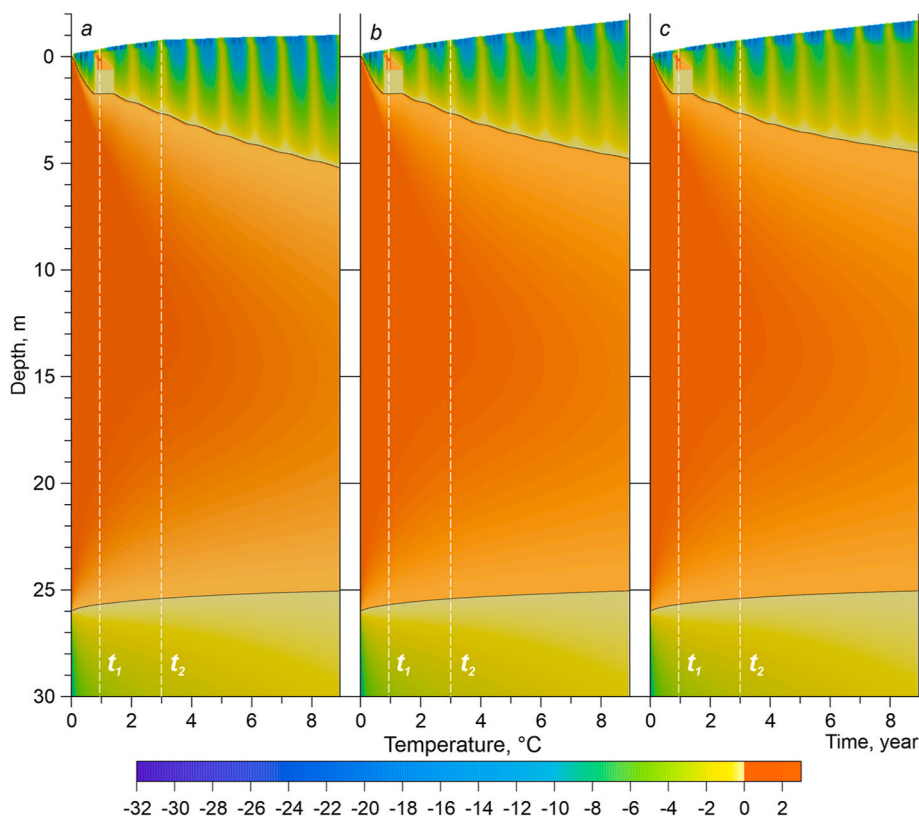
Fig. 11. Results of scenario calculations No. 1 (a), 2 (b), and 3 (c) of Lake Dålk development for the next 5 years.

thickness, but the density of snow fallen during the year increases uniformly from 110 kg/m³ (corresponding to freshly fallen snow (Sosnovsky, 1984, 2006; Osokin et al., 1999)) to the value obtained from the core and equal to 462 kg/m³. The simulation results Fig. 11c show that the ice thickness over Lake Dålk by the end of the fifth calculation year increased only to 5.06 m (the increase since the time t_2 was 1.99 m). That is, the rate of freezing is expected to be even slower. The bottom of Lake Dålk had also frozen a total of 0.97 m by the end of 2028. This demonstrates once again that the processes occurring on the surface of the reservoir do not contribute significantly to its freezing from the bottom. The total decrease in the depth of Lake Dålk under the given scenario for the entire calculation period reached 6 m. This is 22.5% of the initial depth.

It should be noted that the latter scenario is the most realistic. It involves cyclic snowfall followed by firnization. As can be seen from all of the presented scenarios, for the time interval from t_2 to the end of the calculation period, the calculation results for the values differ from each other by about a third (30%).

Thus, if the current dynamics continue, we can expect Lake Dålk to be completely frozen over in about 40–45 years. In addition, repeated outbursts of this reservoir are possible only if there is an additional inflow of water masses from neighboring lakes. In its absence, the lake will gradually degrade.

5. Conclusions

As a result of the studies performed, the actual boundaries of the englacial Lake Dålk were determined. According to GPR data, the lake is currently communicating with a small rock lake.

The thickness of ice 3 years after the formation of the Lake Dålk varies from 2 to 6.2 m. There is also a tendency to increase the ice thickness in the marginal part of the reservoir adjacent to the Dålk Glacier. Core drilling showed stratigraphic and thermal homogeneity of the lake ice. According to the results of isotope analysis, we can assume

that the ice was formed in an open system, i.e., water exchange took place during ice formation in the englacial lake.

As a result of one-dimensional mathematical modeling, 3 scenarios of further lake evolution have been demonstrated. For all scenarios, we can expect Lake Dålk to be completely frozen over in about 40–45 years, if the current dynamics persist. Repeated outbursts of this reservoir are possible only in the presence of an additional inflow of water masses from neighboring lakes, which is also likely, given the history of the formation of the expect Lake Dålk.

Declaration of competing interest

The authors declare that they have no known competing financial interests or personal relationships that could have appeared to influence the work reported in this paper.

geophysical and geodetic equipment and assistance in its preparation for field work, AARI LICOS employee A.V. Kozachek for laboratory measurements of isotope composition.

References

Boronina, A., Popov, S., Pryakhina, G., Chetverova, A., Ryzhova, E., Grigoreva, S., 2021. Formation of a large ice depression on Dålk Glacier (Larsemann Hills, East Antarctica) caused by the rapid drainage of an englacial cavity. J. Glaciol. 67 (266), 1121–1136. https://doi.org/10.1017/jog.2021.58.

Boronina, A.S., 2022. Large-scale outbursts of lakes in the Antarctic oases: current knowledge. Ice Snow 62 (1), 141–160. https://doi.org/10.31857/S2076673422010122 [In Russian].

Chernyak, G.Y., 1987. Electromagnetic Methods in Hydrogeology and Engineering Geology. Nedra, Moscow [In Russian].

Craig, H., 1961. Isotopic variations in meteoric waters. Science 133, 3465. https://doi.org/10.1126/science.133.3465.1702.

Gasparon, M., Lanyon, R., Burgess, J.S., Sigurdsson, I.A., 2002. The freshwater lakes of the Larsemann Hills, east Antarctica: chemical characteristics of the water column. In: ANARE Reports, vol. 147. Australian Antarctic Division.

Gibson, J.J., Prowse, T.D., 1999. Isotopic characteristics of ice cover in a large northern river basin. Hydrol. Process. 13 (16), 2537–2548. https://doi.org/10.1002/(SICI)1099-1085(199911)13:16<2537::AID-HYP940>3.0.CO;2-A.

Gillieson, D., Burgess, J., Spate, A., Cochrane, A., 1990. An Atlas of the Lakes of the Larsemann Hills, Princess Elizabeth Land, Antarctica, vol. 74. ANARE Research Notes. Antarctic Division Australia.

Glazovsky, A.F., Macheret, Y.Y., 2014. Water in Glaciers. Methods and Results of Geophysical and Remote Sensing Studies. GEOS, Moscow [In Russian].

Grigoreva, S.D., Kiniabaeva, E.R., Kuznetsova, M.R., Popov, S.V., Kashkevich, M.P., 2021. Structure of snow-ice dams of the outburst lakes in the Broknes Peninsula (Larsemann Hills, East Antarctica) based on ground-penetrating radar data. Ice Snow 61 (2), 291–300. https://doi.org/10.31857/S2076673421020089 [In Russian].

Kaup, E., Burgess, J., 2002. Surface and subsurface flows of nutrients in natural and human impacted lake catchments on Broknes, Larsemann Hills, Antarctica. Antarct. Sci. 14, 4. https://doi.org/10.1017/S0954102002000123.

Martos, Y.M., Catalán, M., Jordan, T.A., Golynsky, A., Golynsky, D., Eagles, G., Vaughan, D.G., 2017. Heat flux distribution of Antarctica unveiled. Geophys. Res. Lett. 44, 11 417–11 426. https://doi.org/10.1002/2017GL075609.

Osokin, N.I., Samoilov, R.S., Sosnovskii, A.V., Sokratov, S.A., Zhidkov, V.A., 1999. On estimation the influence of snow cover characteristics variability on soils freezing. Earths Cryosphere 3 (1), 3–10 [In Russian].

Popov, S., 2022. Ice cover, subglacial landscape, and estimation of bottom melting of Mac. Robertson, Princess Elizabeth, Wilhelm II, and western Queen mary lands, east Antarctica. Rem. Sens. 14 (1), 241. https://doi.org/10.3390/rs14010241.

Popov, S., Boronina, A., Pryakhina, G., Grigoreva, S., Sukhanova, A., Tyurin, S., 2018. Breakthroughs of glacial and subglacial lakes at the Larsemann Hills (east Antarctica) in 2017-2018. Georisk 7 (3), 56–67 [In Russian].

Popov, S.V., 2017. Determination of permittivity on diffraction curve for the model of inclined layered medium. Earths Cryosphere 21 (3), 83–87. https://doi.org/10.21782/KZ1560-7496-2017-3(83-87 [In Russian].

Popov, S.V., Boronina, A.S., Nemchinova, A.V., Lebedeva, L.S., Biryukov, A.S., 2023. Formation of subaerial taliks in Larsemann Hills, Princess Elizabeth land, east Antarctica. Polar Sci. (in review).

Popov, S.V., Pryakhin, S.S., Bliakharskii, D.P., Pryakhina, G.V., Tyurin, S.V., 2017. Vast ice depression in Dålk Glacier, east Antarctica. Ice Snow 3 (57), 427–432. https://doi.org/10.15356/2076-6734-2017-3-427-432.

Samarsky, A.A., Vabishchevich, P.N., 2003. Computational Heat Transfer. Editorial URSS, Moscow, p. 784 [In Russian].

Shevnina, E., Kourzeneva, E., 2017. Thermal regime and components of water balance of lakes in Antarctica at the Fildes peninsula and the Larsemann Hills. Dyn. Meteorol. Oceanogr. 69 (1), 1317202 https://doi.org/10.1080/16000870.2017.1317202.

Sosnovsky, A.V., 1984. Calculation of the optimal thickness of the water-ice mixture layer during ice freezing over large areas. Data Glaciol. Stud. 50, 223–231 [In Russian].

Sosnovsky, A.V., 2006. Mathematical modelling of the influence of snow cover thickness on degradation of permafrost at climate warming. Earths Cryosphere 10 (3), 83–88 [In Russian].

Sukhanova, A.A., Popov, S.V., Boronina, A.S., Grigorieva, S.D., Kashkevich, M.P., 2020. Geophysical surveys in the vicinity of the Progress Station, East Antarctica, performed during the 63rd RAE season (2017/18). Ice Snow 60 (1), 149–160. https://doi.org/10.31857/S2076673420010030 [In Russian].

Vieira, G., Bockheim, J., Guglielmin, M., Balks, M., Abramov, A.A., Boelhouwers, J., Cannone, N., Ganzert, L., Gilichinsky, D.A., Goryachkin, S., López-Martínez, J., 2010. Thermal state of permafrost and active-layer monitoring in the antarctic: advances during the international polar year 2007–2009. Permafr. Periglac. Process. 21 (2), 182–197. https://doi.org/10.1002/ppp.685.

Vladov, M.L., Starovoitov, A.V., 2004. Introduction to Ground-Penetrating Radar. Moscow State University, Moscow [In Russian].